blueEpidemic local final size in a metapopulation network as indicator of geographical priority for control strategies in SIR type diseases

U.J. Giménez-Mujica[a], A. Anzo-Hernández[b], J. Velázquez-Castro[a]

[a] Facultad de Ciencias Físico-Matemáticas,
Benemérita Universidad Autónoma de Puebla,
Avenida San Claudio y 18 Sur, Colonia San Manuel, 72570.
Puebla, Puebla, México.

[b] Cátedras CONACYT - Benemérita Universidad Autónoma de Puebla - Facultad de Ciencias Físico-Matemáticas,
Benemérita Universidad Autónoma de Puebla,
Avenida San Claudio y 18 Sur, Colonia San Manuel, 72570.
Puebla, Puebla, México.

Abstract

The main limitation blueon designing epidemic control strategies bluelies in their economic and social costs. Thusblue, a practical and efficient approach takes into consideration these factors. Most epidemics evolve in a structured population, bluebeing the geographical structure the most evident. In this situation, bluehaving a criteria bluefor identifying the most effective locations where control measures bluecan optimize available resources blueis desirable. In this paper, a regional index based on the final blueepidemic size predicted by a metapopulation model is proposed. An efficient algorithm to calculate explicit blueindex values was developed, and different control strategies that used the recommended index were compared with others that do not take bluethe index information into account. We found that the proposed index bluerepresents an easy and fast criterion to guide simple control strategies. This bluetype of index blueoffers a new powerful approach where the information encoded in a deter-

Email addresses: uvencioj@gmail.com (U.J. Giménez-Mujica), andres.anzo@hotmail.com (A. Anzo-Hernández), jorge.velazquezcastro@correo.buap.mx (J. Velázquez-Castro)

ministic mathematical model can be summarized to guide realistic and practical control strategies bluefor disease bluespreading and epidemics.

Keywords: Mathematical epidemiology, epidemic final size, SIR meta-population model, selecting controlling patches.

1. Introduction

At present, bluehuman-to-human transmitted diseases (influenza, H1N1, measles, blueSARS-CoV2) bluerepresent a primary concern in most countries (Fraser et al. (2009)), bluesince a large part of the population is liable to catch them, turning these diseases into a recurring threat worldwide. An epidemic outbreak of these kind typically bluespreads over broad geographical areas where many zones of different social and environmental characteristics are affected (Lee et al. (2018); Angelo et al. (2019)). The most conspicuous and recent example is the propagation of blueSARS-CoV2 that resulted in a pandemic. The extended nature of an epidemic leads to a structured and blueinhomogeneous spread of the disease among the affected zones (Chinazzi et al. (2020)). This structured evolution of the disease bluedevelops not only spatially, but also in time, affecting some zones first and then propagating to other regions in complex ways (Lee et al. (2012)). The complex propagation of bluea disease bluecomplicates the desing of efficient control strategies bluewhere economic and human resources are limited. A natural approach would be to bluedetermine where to apply control strategies in order to minimize the potential impacts that epidemics can cause. This approach would require real-time information blueregarding the spread of the disease bluein each affected zone, bluethus demanding human and economic resources. A more straightforward approach would be bluehaving each zone labeled by an index that blueidentifies its potential blueimpacts due to the pandemic. By blueidentifying the bluerelevance of the disease severity in a specific zone, it is possible to direct the available resources for prevention measures and control strategies to the most potentially affected sites.

blueThe epidemic final size, a term developed in the context of mathematical epidemiology, is essential to measure the severity of the pandemic (Brauer et al. (2019); Martcheva (2015); Miller (2012); Magal et al. (2018)). Previous studies (Brauer et al. (2019); Martcheva (2015); Miller (2012)) have calculated bluethe epidemic final size using models blueonly for homogeneously mixed populations. In order to overcome this limitationblue, modeling epidemics on metapopulation networks blueproves useful (Colizza & Vespignani (2008); Balcan & Vespignani (2012); Pastor-Satorras et al. (2015)). The blueutilization of metapopulation networks to model epidemics allows us to describe a more realistic scenario at the cost of increasing bluetheir mathematical complexity. Although bluecomputer technology to solve these problems numerically currently exists, in practice, the resulting models may consist of hundreds of equations. blueThat is the case, for instance, when patches blueare used to represent cities, or, even more, bluepostal code. blueIn these situations, an efficient algorithm will help to reduce both memory and CPU usage.

The complexity of this type of model can be used to analyze the components that describe their dynamics bluemore efficiently. This allows us to generalize some traditional concepts of epidemiology. In particular, bluewe understand the final size of the disease blueas a single quantity in models describing a single group. However, in (Magal et al. (2018)), a multi-group model is used in order to calculate the total bluenumber of infected individuals in each separate group. Analogous bluefinding have been registered in metapopulation models, where there is a final size of the disease for each patch in addition to the entire system's final size. The bluemulti patch final size has been previously addressed for some stochastic models in (Miller (2012)), where relevant quantities are provided in terms of an blue*a priory* individual's infection probability.

In this paper, we blueconsider the final size for a single patch blueas the local final size of the disease, and the final size of the entire system blueas the final global size. blueTaking the final size of the disease blueas a way to measure the epidemic severity, we propose that the set of local final sizes of the disease in a metapopulation model can guide some control strategies.

The control strategies that can be designed bluewith the information blueof the set of local final sizes aim to reduce bluethe disease impact in most affected areas in a highly connected context. It is worth bluenoting that the aim of these strategies is different from other more common control strategies, bluewhich is to reduce total cases regardless of the local severity in different regions.

In this article, we propose a SIR model in a metapopulation network described bluethrough differential equations. We deduct the set of local final sizes of the disease blueanalytically. The obtained mathematical expression implicitly provides the actual value of the final size. blueIn this manner, we develop an efficient algorithm to calculate the final size values. We then supply a criterion based on the final size bluein order to to select the patches blueand apply local control. The guided control strategy will be compared with a strategy of control for randomly selected patches. This comparison will help to corroborate the benefits of a guided strategy in contrast with a random strategy.

This article is organized as follows: in section 2, we describe the SIR epidemic model in networked populations connected by human mobility. blueThen, we analytically derive the epidemic final size expression. In section 3, we describe the proposed iterative algorithm to estimate the final epidemic size in each patch. In section 4, we propose a criterion to select the controlling patch. In section 5, we bluenumerically illustrate the effectiveness of the algorithm by comparing two different types of network structures. blueFinally, in section 6 we present bluethe conclusions.

2. Epidemic final size in a networked population.

We consider a human population, geographically located at n distinguishable regions called patches, and connected by the mobility of individuals. We assume that each patch is inhabit by a well-mixed population of size N_i, where the subindex $i \in \{1, ..., n\}$ represents the patch label. Let, respectively, $S_i(t)$, $I_i(t)$ and $R_i(t)$ the number of susceptible, infected and recovery residents from patch i at time instant t; such that $N_i = S_i(t) + I_i(t) + R_i(t)$ remains constant all the

time.

Based on the Lagrangian modeling approach (Bichara et al. (2015); Velázquez-Castro et al. (2018)), the mobility of individuals among patches is described by the residence-time matrix $P = (p_{ij})_{i,j=1}^{n}$ whose entries satisfy:

$$0 \leq p_{ij} \leq 1\,; \quad \text{and} \quad \sum_{k=1}^{n} p_{ik} = 1 \quad \forall i, j\,; \tag{1}$$

where p_{ij} describes the fraction of time that residents from patch i spend in patch j. It is worth noting that the matrix P represents a network of patches connected by directed and weighted links. In blueFigure (1) we show an example of a networked population and its corresponding residence-time matrix.

Due to mobility, the effective number of individuals already present in patch i is given by $w_i = \sum_{j=1}^{n} p_{ji} N_j$; where the fraction of N_i residents that remains in its own patch is given by $p_{ii} N_i$; and the fraction of N_j neighboring residents that daily visit patch i is $p_{ji} N_j$, with $j = 1, \ldots, n$. In this context, the inflow of infected visitors on patch k is given by:

$$\mathcal{F}_k = \frac{1}{w_k} \sum_{j=1}^{n} p_{jk} I_j\,; \tag{2}$$

which embody both the fraction of infected individuals coming from neighboring patches and the own infected in patch k. Then, the disease dynamics in the networked population is described by the following set of $3n$ ODE's:

$$\dot{S}_i = -\sum_{k=1}^{n} \beta^k (p_{ik} S_i) \mathcal{F}_k\,, \tag{3}$$

$$\dot{I}_i = \sum_{k=1}^{n} \beta^k (p_{ik} S_i) \mathcal{F}_k - \gamma_i I_i\,, \tag{4}$$

$$\dot{R}_i = \gamma_i I_i\,, \tag{5}$$

for $i = 1, \ldots, n$; the parameter $\gamma_i > 0$ describes the recovery rate of infected residents from patch i and, β^k is the risk of infection in patch i.

We define the initial condition in each patch as follows: $S_i(0) = N_i$, $I_i(0) = 0$, $R_i(0) = 0$ for $i = 2, \ldots, n$; and $S_1(0) = N_1 - 1$, $I_1(0) = 1$, $R_1(0) = 0$. That is,

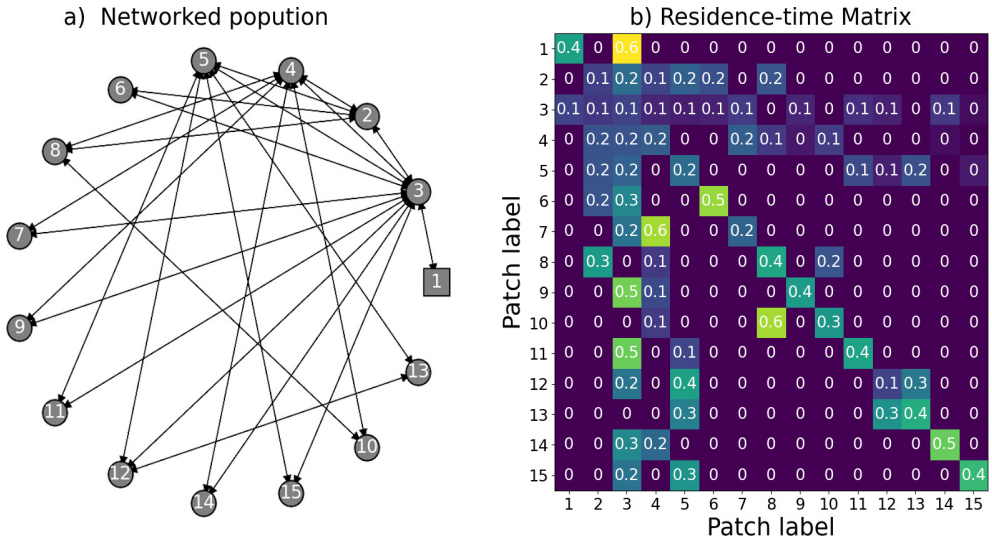

Figure 1: a) An example of a networked population where each node is a geographical region called patch inhabited by a well-mixed population, and where the directed links represent the individuals mobility among patches (the square node represents the patch where the outbreak started). b) The corresponding representation of the residence-time matrix, whose entries p_{ij} describes the proportion of time that residents from patch i spend in patch j and satisfy Eq. (1).

by convention, we assume that at the beginning of the epidemic the patch with label $k = 1$ has a single infected resident, while the other patches are populated by susceptible individuals.

By substituting $\mathcal{F}_k$ (Eq. (2)) into the Eqs. (3)-(5), the SIR epidemic model in a networked population can be rewritten as:

$$\dot{S}_i = -S_i \sum_{j=1}^{n} \beta_{ij} I_j \,, \tag{6}$$

$$\dot{I}_i = S_i \sum_{j=1}^{n} \beta_{ij} I_j - \gamma_i I_i \,, \tag{7}$$

$$\dot{R}_i = \gamma_i I_i \,, \tag{8}$$

for $i = 1, \ldots, n$; where the effective risks of infection are given by:

$$\beta_{ij} = \sum_{k=1}^{n} \beta^k \frac{p_{ik} p_{jk}}{w_k}\,; \quad \forall i, j \in \{1, ..., n\}\,. \tag{9}$$

That is, the metapopulation network model described by equations (3)-(5), where a set of separated well-mixed sub-populations is considered, can be rewritten as an epidemic model of a single well-mixed population, where individuals are classified according to their patch of residence; in other words, the system of equations (6)-(8) could be interpreted as a multi-group epidemic model, with β_{ij} the rate contact among residents from patch i and j. It is worth mentioning that the multi-group model (6)-(8) is equivalent to the epidemic model analyzed by Pierre Magal *et. al* in (Magal et al. (2018)), where human mobility among patches is not considered. In Figure (3) we show an example of the dynamical behavior of the effective SIR epidemic model (6)-(8), with the network topology and residence-time matrix given in Figure (1).

In the context of mathematical epidemiology, the final size is the total proportion of individuals who have been infected during the epidemic (Brauer et al. (2019); Miller (2012)). A common methodology to asses this is through the mathematical expression of the final proportion of recovered individuals $R_i(\infty)/N_i$; i.e., with the explicit solution of the recovery compartment (Eq. (8)) divided by the total population and evaluated the limit as time approaches to infinity.

In order to derive an explicit expression for $R_i(\infty)/N_i$ in each patch, we sum and integrate the susceptibles $S_i(t)$ (Eq. (6)) and infected $I_i(t)$ (Eq. (7)) compartments, and obtain:

$$-\gamma_i^{-1} \int_0^{\infty} \left(\dot{S}_i(t) + \dot{I}_i(t) \right) dt = \frac{N_i - S_i(\infty)}{\gamma_i} = \int_0^{\infty} I_i(t) dt\,; \tag{10}$$

where we have used:

$$I_i(\infty) = \lim_{t \to \infty} I_i(t) = 0\,, \quad \text{and} \quad N_i = S(0) + I(0) \quad \forall i. \tag{11}$$

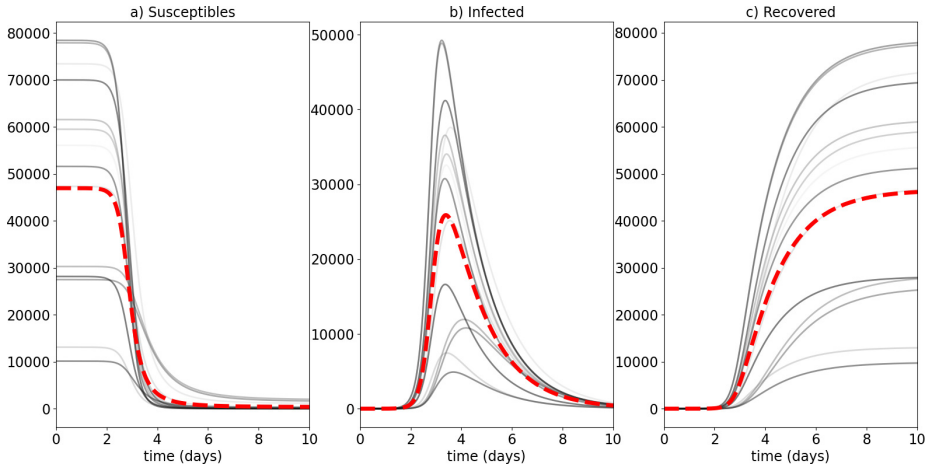

Figure 2: Dynamical behavior of the SIR epidemic model in a networked population (6)-(8). The dashed red curve represents the mean value over the patches trajectories. The population sizes N_i, and the patch risk of infection β^i, for $i = 1, \ldots, 15$ are uniformly random selected in the ranges $[10,000, 30,000]$ and $[1.5, 2.5]$ respectively; the recovery rate $\gamma_i = 0.7$ for all patches.

On the other hand, we obtain from Eq. (6) and Eq. (10) :

$$\log\left(\frac{S_i(0)}{S_i(\infty)}\right) = \sum_{j=1}^{n} \beta_{ij} \int_0^\infty I_j(t)dt = \sum_{j=1}^{n} \beta_{ij} \frac{N_j - S_j(\infty)}{\gamma_j}\,, \tag{12}$$

then $S_i(\infty) = S_i(0)e^{-\theta_i}$; where

$$\theta_i(S_1, \ldots, S_n) = \sum_{j=1}^{n} \beta_{ij} \frac{N_j - S_j(\infty)}{\gamma_j}\,, \quad \text{for} \quad i = 1, \ldots, n\,. \tag{13}$$

The functions $\theta_i(S_1, \ldots, S_N)$ determines the total number of new infections generated in patch i caused by infected travelers who visit such patch.

Since $N_i = S_i(t)+I_i(t)+R_i(t)$ remains constant all the time and, by Eq. (11), when $t \to \infty$ we get that $R_i(\infty) = N_i - S_i(\infty)$. Then, the explicit expression for the epidemic final size in a given path i is

$$R_i(\infty)/N_i = 1 - S_i(0)e^{-\theta_i}/N_i\,. \tag{14}$$

Note that, although blueEq. (14) gives an explicit form of the final size of

the epidemic for each patch, solving it analytically represents a problem of great difficulty due to its implicit dependence on the terms $S_1(\infty), \ldots, S_n(\infty)$.

In the next sectionblue, we propose an iterative algorithm to estimate the value of Eq. (14).

3. Iterative algorithm to calculate the epidemic final size in each path.

One of the main difficulties in evaluating the epidemic final size in a given patch i with Eq. (14), lies in the implicit dependence on $S_1(\infty), \ldots, S_n(\infty)$ of the function θ_i (Eq. (13)). That is, it requires to know the analytical solution of the SIR epidemic model (6)-(8) and evaluate the limit as time goes to infinity. To answer this problem, we propose to rewrite Eq. (14) as a set of difference equations, such that after iterating it a given number of time steps, we obtain the value of $R_i(\infty)$, for $i = 1, \ldots, n$.

Let $x_i^k \in \mathbb{R}^+$ a set of continuous variables representing the number of infected individuals in patch i at discrete time step $k \in \mathbb{N}$. Based on Eq. (14) multiplied on both sides by N_i, we propose the following set of n difference equations which describes the evolution of variables x_i^k:

$$x_i^{k+1} = f_i(x_1^k, \ldots, x_n^k) = N_i - S_i(0)e^{-\theta_i^k}, \quad \text{for} \quad i = 1, \ldots, n; \tag{15}$$

where $f_i : \mathbb{R}^n \longrightarrow \mathbb{R}$ is a differentiable map, and

$$\theta_i^k \equiv \theta_i^k(x_1^k, \ldots, x_n^k) = \sum_{j=1}^{n} \beta_{ij} \frac{x_j^k}{\gamma_j}, \quad \text{for} \quad i = 1, \ldots, n. \tag{16}$$

By defining the vector $X^k = (x_1^k, \ldots, x_n^k)^T \in \mathbb{R}^n$, the set of differences equations (15) could be expressed in compact form as:

$$X^{k+1} = F(X^k); \tag{17}$$

with $F(X^k) = (f_1(X^k), \ldots, f_n(X^k))^T \in \mathbb{R}^n$. For a given initial condition X^0, a solution of (17) is a real sequence $(X^m)_{m\in\mathbb{N}}$, that satisfies blueEq. (17) for $m \geq 0$. In blueFigure (3) we show the evolution of the variables x_i^k for the networked

population presented in blueFigure (1.a) (and the corresponding residence-time matrix show in blueFigure (1.b). A sample of three variables are shown in this figure in order to illustrate the convergence of blueEq. (17) after ten iterations, approximately, and setting the initial condition as $X^0 = (1, \ldots, 1)^T$. The red dashed lines in blueFigure (3) are the corresponding values of the recovery compartment evaluated in the limit as time goes to infinity $R_i(\infty)$; which is evaluated by solving numerically the SIR epidemic model (6)-(8) and extract the last value of the time series of the recovery compartment (See blueFigure (3.c)). That is, we can corroborate numerically, that the set of difference equations (15) convergence to the value of $R_i(\infty)$ which when dividing by N_i, gives us the desired value of the epidemic final size. The following proposition guarantees the convergence of blueEq. (17).

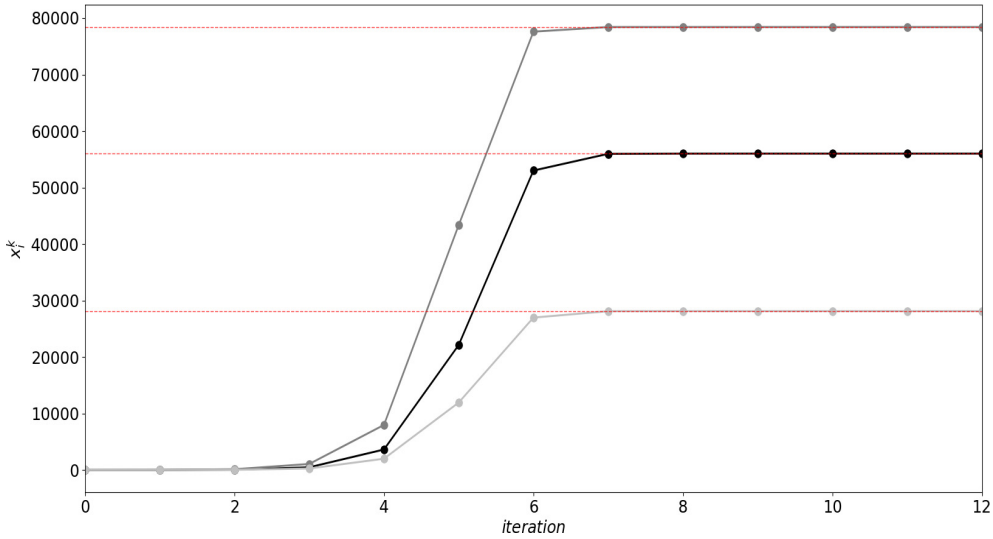

Figure 3: Evolution of the set of difference equations (15) for the networked population shown in blueFigure (1). For this figure a sample of the dynamics of three variables are shown in order to better illustrate the convergence of the equations when the initial condition is setting as $X^0 = (1, \ldots, 1)^T$. The red dashed lines are the corresponding values of $R_i(\infty)$ taking from the numerical solution of the SIR epidemic model (6)-(8).

Proposition 1. *Let $F : \mathbb{R}^n \longrightarrow \mathbb{R}^n$ a differentiable map of the form*

$$F(X^k) = (N_1 - S_1(0)e^{-\theta_1^k}, \cdots, N_n - S_n(0)e^{-\theta_n^k})^T ;$$

with $X^k = (x_1^k, \ldots, x_n^k)^T \in \mathbb{R}^n$ and, $\theta_i^k \equiv \theta_i^k(x_1^k, \cdots, x_n^k) = C_1 x_1^k + \cdots + C_n x_n^k > 0$, $\forall i \in \{1, ..., n\}$; with $\{C_l\}_{l=1}^n$ a set of positive constants. Let $X^{k+1} = F(X^k) = F^{k+1}(X^0)$ the $(k+1)$-th iteration of the map F, with $k \in \mathbb{N}$; $X^0 \in \mathbb{R}^n$ the initial condition and, $F^k(X^0) \equiv F \circ \cdots \circ F(X^0)$ the k times composition of $F(X^0)$. If $X^0 = (1, \cdots, 1)^T \in \mathbb{R}^n$, then the solution of the difference equation (17) converges.

The proof of proposition (1) can be consulted in Appendix A. In general, we demonstrate by induction, that each entry i of X^k is bounded superiorly by N_i, and are monotonous increasing, from analysis in $\mathbb{R}$ in metric spaces and the fact that a sequence in $\mathbb{R}^n$ converges if at each input i the ordered sequence converges, we proof that the sequence $(X^m)_{m\in\mathbb{N}}$, with $m \geq 1$, converges. It is worth mentioning that when Eq. (14) has a unique solution, the proposition (1) converges to the limit $R_i(\infty)$, for $i = 1, \ldots, n$.

Based on the set of difference equations (15) we propose the following algorithm to calculate the epidemic final size in each patch:

Algorithm 1: Iterative algorithm to calculate the epidemic final size.

Input: $\{N_i, S_i(0), \beta^i, \gamma_i\}_{i=1}^n$; $P = (p_{ij})_{i,j=1}^n$.

Output: $\{R_1(\infty)/N_1, \ldots, R_n(\infty)/N_n\}$.

Data: Setting $X^0 = (1, \cdots, 1)$.

for $k \in [0, m]$ **do**

  $X^{k+1} = F(X^k) = F^{k+1}(X^0)$

Data: Setting $R_i(\infty)/N_i = X_i^m/N_i$.

Where $m \in \mathbb{N}$ is the number of iterations and, X_i^m is the i-th entry of the vector X^m. It is worth remarking that the above algorithm can be performed in few blueiterations, which means that it could be numerically implemented with little computational cost; and it does not require to solve the set of equations numerically or analytically (6)-(8).

Remark: Theories as fixed point could be considered to demonstrate the existence and uniqueness of solutions to Eq (14). For example, P. Magal *et.al* in Magal et al. (2018) have used this theory to demonstrate the existence and uniqueness of the set of difference equations (14); but, unlike our working hypotheses, P. Magal considers an irreducible transmission; that is, the matrix, whose entries are given by parameters β_{ij}, is irreducible non-negative. In Appendix B we discuss a methodology to rewrite Eq. (14) as an equivalent fixed point problem without imposing any restriction to the matrix composed of parameters β_{ij}. Furthermore, we present a theorem that could be used to guarantee the existence and uniqueness of the solution of Eq. (14). Since this problem is out of the scope of this work, we leave them indicated as an open problem for future research works.

In the following section we use the above proposed algorithm to select patches where a control protocol can reduce the number of infected individuals on the entire network.

4. Criterion to select controlling patches and control protocols.

Given the residence-time matrix P, the number of inhabitants in each patch N_i, the risk of infection β_i and the recovery rate γ_i, the algorithm 1 blueallows us to calculate the total proportion of individuals that will become infected in each patch. That is, with the set of difference equations proposed in blueEq. (15), we can know *a priori* bluewhich patches will have the maximum number of infected inhabitants. blueWith this information, it is possible to design a control protocol over specific patches instead of blueimplementing a reactive selection of the controlling patches, where the control is applied randomly as outbreaks appear on the patches.

blueAs our main hypothesis, we propose that by controlling the patches with the highest $R_i(\infty)$ bluevalue, calculated after iterating blueEq. (15), blueit is possible to reduce the number of infected individuals blueinside the network and bluein the most affected patch. In order to corroborate bluethis hypothesis,

we propose and compare two forms of controlling patches selection: random, and targeted. For bluethe latter, we use two indexes to guide the selection. The absolute final size index (AFS) blueis defined as the maximum over the set $\{R_1(\infty), \ldots, R_n(\infty)\}$, and the relative final size index (RFS) blueis defined as the maximum over the set $\{R_1(\infty)/N_1, \ldots, R_n(\infty)/N_n\}$. blueIn other words, the RFS index takes into account the proportion of infected individuals in each patch.

blueWe also propose as control protocol reducing the risk of infection β_i in the selected patch i. This bluereduction is the most common form of control in mathematical epidemiology, and it is usually related blueto the implementation of social measures, bluesuch as quarantine, school and workplace closures, campaigns to promote physical distancing bluebetween individuals, hand hygiene, wearing mask, isolating patients, among others measures. This form of control is modeled via a control parameter $u \in [0, 1]$, which is introduced into the SIR model (6)-(8) as follows:

$$\dot{S}_i = -S_i \sum_{j=1}^{n} (1 - u\delta_i)\beta_{ij} I_j \,, \tag{18}$$

$$\dot{I}_i = S_i \sum_{j=1}^{n} (1 - u\delta_i)\beta_{ij} I_j - \gamma_i I_i \,, \tag{19}$$

$$\dot{R}_i = \gamma_i I_i \,, \tag{20}$$

where $\delta_i = 1$, if the patch with index i is the selected patch to be controlled, and $\delta_i = 0$, blueif otherwise.

blueUsing the above protocol and the two proposed strategies to select the patches to be controlled (random and targeted), in the next section, we analyze and compare the following scenarios numerically:

- blueThe disease spread over a networked population that does not apply any control protocol.
- blueThe disease spreads over a networked population where control is applied to a random selected patch.

- blueThe disease spreads over a networked population where control is applied by selecting the patch with the aid of the AFS or RFS index.

blueThese simulated strategies are intended to show and compare whether the AFS and RFS indexes could serve as reliable indicators of which patches are more convenient to control. The protocol indicates that a single patch must be controlled to observe its effects; however, this does not account for a complete control strategy proposal.

5. Numerical examples

Recent studies in the field of complex networks blueagree that networks such as cities, airports, traffic flows, blueand other urban systems evidence the small-world (Ding (2019); Volchenkov & Blanchard (2008); Mansilla & Mendozas (2010)) and the scale-free effect. The first effect is characterized by the presence of links that reduce the distance among nodes, which we call bridging links. blueThe second effect is identified by the presence of highly connected nodes called hubs. A remarkable example of a network with hubs is the blueairport network (Guida & Maria (2007)). In order to illustrate the use of the AFS and RFS indexes as criteria to select the controlling patch, we use two different algorithms to construct graphs with bridging links and hub nodes.

The first type of graph we consider is constructed with the algorithm proposed by M. E. J. Newman and Duncan Watts (Newman & Watts (1999)). blueWe denote the graph constructed bluewith this algorithm blueas NWG. The first step in the algorithm is to generate a regular graph (*i.e.*, a graph where the nodes have the same number of connections). blueThen an extra link (usually referred to as bridging link) is added between pairs of nodes with independent probability p. blueThese bridging links reduce the shortest path length of the NWG, understanding path lengt as the smallest number of links in a path that connect any pair of nodes.

The second type of graph we consider is generated with the algorithm proposed by Albert-Lázló Barabásis and Réka Albert (Barabási & Albert (1999)).

Parameter	Description	value
N_i	Population size	[10.000 , 1.000.000]
γ_i	Effective recovery rate	0.7
β^i	Effective infection rate	[1.5 , 2.5]
u	Control parameter	0.5

Table 1: blueIn each simulation, for $i = 1, \ldots, 15$, N_i is chosen randomly with a normal distribution, in order to model a network with large and small populations while the choice of β^i for each simulation, it is also chosen randomly with a normal distribution.

blueWe denote bluethe graph constructed with this algorithm as BAG. The algorithm begins with an initial number of connected nodes, bluethen, new nodes are added to the network iteratively. Each new node connects with m already present nodes in the network following the preferential attachment principle. One of the main structural features of a graph constructed with this algorithm is the presence of hub nodes.

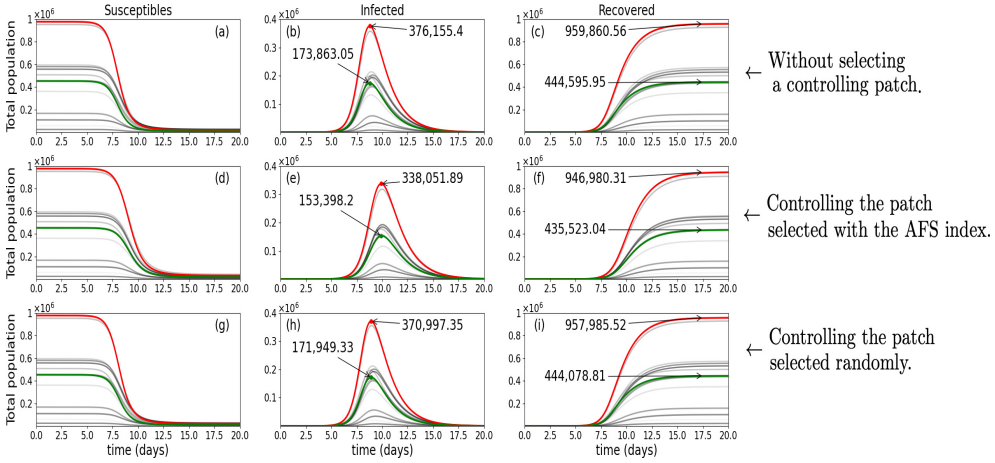

Figure 4: Time series of the SIR model (18)-(20) in a NWG and selecting the controlling patch with the AFS index. Red line represent the patch selected with the AFS index and green line the patch selected randomly. The dynamics without control are in blueFigures (a), (b) and (c); by selecting the controlling patch with the AFS index are in blueFigures (d), (e) and (f); and by selecting the controlling patch with a random strategy in blueFigures (g), (h) and (i).

For each one of these graphs, we perform an ensemble of one hundred numerical simulations, where, for each simulation run, bluewe solve the system of equations blue(18)-(20) with a new NWG or BAG realization constructed with the parameters NWG $p = 0.3$ and BAG $m = 2$. blueIn Table(1), we describe each epidemiological parameter interpretation and its reference value. Later, to define the residence-time matrix P, we model two possible scenarios: blueone of high mobility, where the parameters p_{ij} are randomly chosen bluewithin the range of $[0, 1]$ and, blueone of low mobility where values for $p_{ii} > 0.7$ are randomly chosen, which implies a low population mobility between patches and a higher fraction of time in its own patches. Next, for each simulation run, we bluenumerically solve the model (18)-(20) three times. blueFor the first one, we do not control any patch. blueFor the second one, we select the controlling patch with the AFS or RFS index. blueFinally, for the third simulation, we bluerandomly select the controlling patch with uniform distribution. blueThe value of the control parameter u is included in Table (1).

In blueFigure (4), we show an example blueof the epidemic dynamics in a NWG from the ensemble of numerical simulations with high mobility. We select the controlling patch with the AFS index. In each row, we display the time series of the SIR model (18)-(20) bluewith no control (blueFigures (4.a), (4.b) and (4.c)), blueby controlling the patch selected with the AFS index (blueFigures (4.d), (4.e) and (4.f)), and blueby controlling the patch randomly selected (blueFigures (4.g), (4.h) and (4.i)).

It is worth noting that blueby applying no control, the peak of the infected curve for the patch selected with the AFS index (red line in blueFigure (4.b)) reached around $376,000$ blueinfections. When control over bluethis patch is applied, the peak of the infected curve is reduced to bluean approximate of $338,000$ blueinfections (red line in blueFigure (4.e)). blueWhen control is applied to a randomly selected patch, the peak of the infected curve is reduced to around $371,000$ blueinfections (red line in blueFigure (4.h)). Furthermore, we observe that blueby implementing a control protocol to the patch selected with the AFS index, the number of blueinfections can also be reduced in other NWG

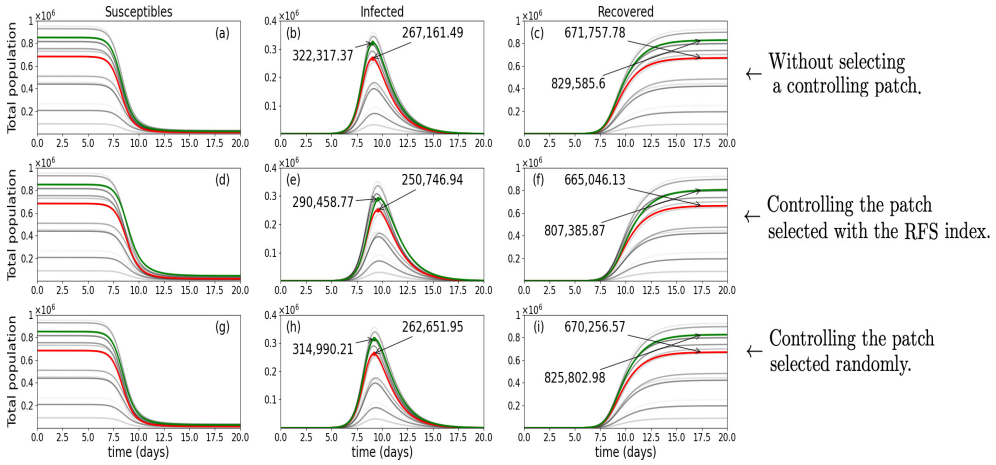

Figure 5: Time series of the SIR model (18)-(20) in a NWG and selecting the controlling patch with the RFS index. Red line represents the patch selected with the RFS index and green line the patch selected randomly. The dynamics without control are in blueFigures (a), (b) and (c); by selecting the controlling patch with the RFS index are in blueFigures (d), (e) and (f); and by selecting the controlling patch with a random strategy in blueFigures (g), (h) and (i).

patches. blueFor example, the peak of the infected curve for the randomly blue-selected patch reached around $174,000$ blueinfections when no control is applied (green line in blueFigure (4.b)), but when a control protocol is implemented to the patch selected with the AFS index, the peak of the infected curve for the bluerandomly selected patch reaches to around $153,000$ blueinfections (green line in blueFigure (4.e)). blueIf the control is applied over bluethis randomly selected patch, the peak of its infected curve reaches around $172,000$ blueinfections (green line in blueFigure (4.h)).

In the context of epidemiology, a public health strategy to control an epidemic outbreak is usually quantified by how much it reduces the peak of the infected curve in order blueto no overwhelm hospital capacities. blueFollowing this idea, we use the bluepeak reduction in the controlling patches as a measure bluefor the effectiveness of a selection patch strategy. blueFor each strategy, a different patch is selected to implement the control protocol. Thus, in order to

decide which control strategy is more effective, we compare the joint infections from the controlling patches of both strategies at the blueoutbreak peak. The strategy that reduced more infections in both patches altogether was blueconsidered as the most effective. In this framework, we propose to quantify the effectiveness of the controlling patch selection as follows: let I_1 bluebe the infected curve of the patch selected with the AFS (or RFS) index (red curve in the example of blueFigure (4)), and let I_2 bluebe the infected curve for the patch randomly selected (green curve in the example of blueFigure (4)). Next, we define the sum of the maxima of I_1 and I_2 for each selection strategy, *i.e.*, $\Sigma_{no.ctr}$, $\Sigma_{idx.ctr}$ and $\Sigma_{rnd.ctr}$ are the sum of $max(I_1)$ and $max(I_2)$ bluerespectively, for the cases when no control is applied to any patch, when bluepatches are selected with one of the proposed indexes, and when bluea controlling patch is randomly selected. Then, for a given simulation run in the ensemble we define effectiveness as

$$E_{run} = \begin{cases} 1 \quad if \quad \Sigma_{no.ctr} - \Sigma_{idx.ctr} \geq \Sigma_{no.ctr} - \Sigma_{rnd.ctr} \\ \\ 0 \qquad\qquad\qquad\qquad otherwise \end{cases} \tag{21}$$

If $E_{run} = 1$, the controlling patch selection with the AFS (or RFS) index for the simulation run bluewill be more effective than a random selection, and the opposite bluewill happen if $E_{run} = 0$. For instance, in Figure (4) we observe that $\Sigma_{no.ctr}$ is around $550,000$ (blueFigure (4.b)), $\Sigma_{idx.ctr}$ is around $491,000$ (blueFigure (4.e)) and, $\Sigma_{rnd.ctr}$ is around $543,000$ (blueFigure (4.h)). blueTherefore, $E_{run} = 1$ for this simulation run.

We average the effectiveness measure $\langle E_{run} \rangle$ proposed in (21), bluefor the one hundred simulations generated with the NWG in the high mobility scenario. blueWe observe that, bluefor 59 % of the simulation runs, the effectiveness is $E_{run} = 1$, that is, the patch selection strategy with the index reduces the peak of the infected curves better than a random selection.

blueOn one hand, blueFigure (5) shows an example of the epidemic dynamics when the controlling patch is selected with the RFS index and a high

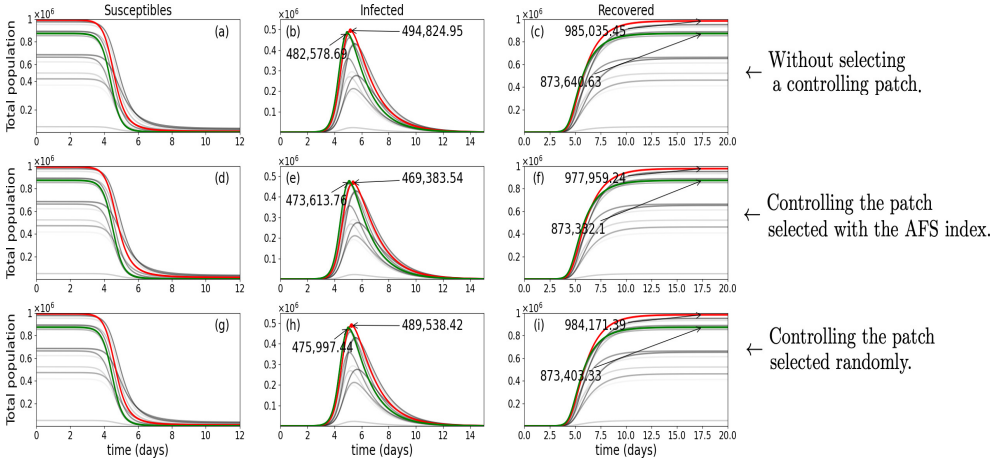

Figure 6: Time series of the SIR model (18)-(20) in a BAG and selecting the controlling patch with the AFS index. Red line represents the patch selected with the AFS index and green line the patch selected randomly. The dynamics without control are in blueFigures (a), (b) and (c); by selecting the controlling patch with the AFS index are in blueFigures (d), (e) and (f); and by selecting the controlling patch with a random strategy in blueFigures (g), (h) and (i).

mobility scenario. It is worth noting that the patch blueselected with the RFS blueindex does not correspond to the path with the highest peak in the infected curve. Furthermore, bluein the example shown in blueFigure (5), the controlling bluerandomly selected patch has a bigger maximum of blueinfections compared to the patch selected with the RFS blueindex. However, the effectiveness of the controlling patch selection is $E_{run} = 1$ in this numerical run since $\Sigma_{no.ctr}$ is around $589,000$ (blueFigure (5.b)), $\Sigma_{idx.ctr}$ is around $541,000$ (blueFigure (5.e)) and, $\Sigma_{rnd.ctr}$ is around $578,000$ (blueFigure (5.h)).

On the other hand, blueFigures (6) and (7) blueillustrate two examples of the epidemic dynamics bluein a networked population with a BAG structure and a high mobility scenario. Both figures show bluetheir respective dynamics when the AFS and RFS blueindexes are used to select the controlling patch. We observe that for these numerical runs, the effectiveness is $E_{run} = 1$. However, Table (2) blueshows that the percentage of cases in which effectiveness equals one

are 53% and 25% for the AFS and RFS indexes respectively bluewhen averaging over the ensemble of simulations. That is, when the network structure is given by the BAG bluein a high mobility scenario, the random selection strategy is more effective than a selection bluemade with our proposed indexes. However, when we perform an ensemble of one hundred bluesimulations run with the BAG in bluea low mobility scenario, we notice (Table (2)) that the effectiveness of our selection strategy blueincreases to 87% and 72%. We also blueobserve an increase in our proposed patch selection strategy when blueperforming an ensemble of run simulations for a NWG in bluea low mobility scenario, (Table (2)).

Another possible strategy bluefor selecting a controlling patch blueconsists in selecting a highly connected patch. blueIn order to analyse this scenario and bluecompare it with a selection strategy guided by the AFS and RFS blueindexes, we perform an ensemble of one hundred run simulations for the NWG and BAG. blueIn this case, instead of selecting a random patch, we select bluea highly connected patch bluefor each run simulation. blueSimilar as before, we perform one hundred simulations for a high mobility bluescenario, and one hundred simulations for a low mobility scenario. Table (2) blueshows the effectiveness average $\langle E_{run} \rangle$ (averaged over the ensemble of simulations). It is worth noting that for a low mobility scenario, the patch selection guided by our proposed indexes is more effective bluethan the highly connected patch selection. blueHowever, selecting the patch with the highest number of connections is more effective bluefor a high mobility scenario (in the sense that, locally, bluethe reduction of the infected curve peak is bigger) than bluedoing the selection with the AFS and RFS indexes.

blue In order to observe the effect on the entire network of the local control, we calculate the peak and the epidemic final size of the entire system in different scenarios. Figure 8 shows the peak of infection when controlling different patches for different values of the control parameter. In Figure 9, the comparison is based on the final size of the epidemic in the entire network.

blueAs can be seen, the proposed control strategies based on the AFS and

RFS indexes outperform even strategies in which the most connected patch is selected for control. This is a nontrivial result that can be explained by the fact that the indexes not only consider the connectivity of the patch, but also the size of the population and the mobility of individuals.

blueIn Figure (8), the maximum of the epidemic in the entire system is also reduced using a strategy based on the proposed index. Thus, finding the place where the control strategy will be optimal can also help controlling the global peak of the epidemic.

blueIn Tables (3) and (4), we can observe some properties of the NWG and BAG networks respectively. Although the most connected patches have a higher degree compared to the patches selected with the proposed indexes, sometimes this is not the most adequate information to select the patch to control. Something similar happens with the clustering measure, where both the most connected patch and those selected with some of the indexes have relatively similar measures in NWG networks. In the case of a BAG network, although this measure does differ from the cases indicated above, it does not provide good information to indicate where the control measure should be applied. Although the betweenness centrality measure indicates that the patches selected by the indexes are not important in terms of network structures, we observe that control measures are more effective when is control is applied. That is, this is not a good indicator to locate where the control measure should be applied. Finally, when observing the topological properties of the patches randomly selected in either NWG or BAG networks, it is evident from Figures (8) and (9), that control will be more effective on the patches selected with the AFS and RFS indexes, even though these properties are similar to those of the patches selected by the proposed indexes. This regards the measures as irrelevant indicators for identifying the best location to apply the control measure in the NWG or BAG networks.

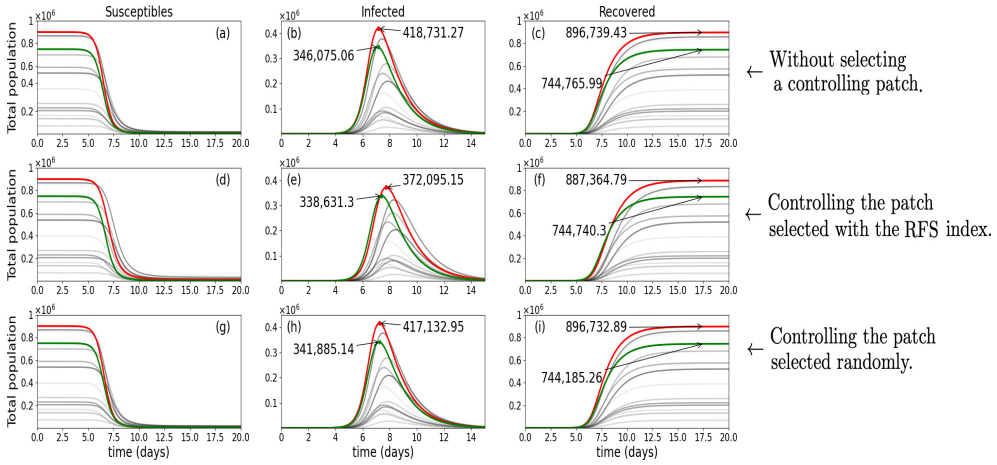

Figure 7: Time series of the SIR model (18)-(20) in a BAG and selecting the controlling patch with the RFS index. Red line represents the patch selected with the RFS index and green line the patch selected randomly. The dynamics without control are in blueFigures (a), (b) and (c); by selecting the controlling patch with the RFS index are in blueFigures (d), (e) and (f); and by selecting the controlling patch with a random strategy in blueFigures (g), (h) and (i).

6. Conclusion

The concept of final size of the epidemic can be generalized to blueencompass structured metapopulatons models bluein order to indicate the local severity blueof an epidemic instead of blueits global severity. Using a mathematical model, an implicit expression for the local final size of the epidemic was found. We propose an iterative algorithm to estimate the epidemic final size in a networked population composed blueof patches connected by the mobility of individuals. The local final size was used to propose control protocols. We use the algorithm as a methodology to select a controlling patch from where blueto apply a control action, bluethus reducing the cases of infected individuals in the network. In this context, with the aim of bluehelping decision-makers to design preventive blue(instead of reactive) control actions, we introduce two indexes: the absolute final size (AFS) index, which takes into account the total final size on each patch, and the relative final size (RFS) index, which considers the local population size. To evaluate the effectiveness of these indexes, we compare three

			Percentage of times that the AFS or RFS index outperforms the other selection strategy.	
Graph	Index	Comparing with patch selection strategy	Low mobility	High mobility
NWG	AFS	random	96 %	59 %
NWG	AFS	highly connected	98 %	39 %
NWG	RFS	random	90 %	40 %
NWG	RFS	highly connected	95 %	19 %
BAG	AFS	random	87 %	53 %
BAG	AFS	highly connected	99 %	21 %
BAG	RFS	random	72 %	25 %
BAG	RFS	highly connected	94 %	3 %

Table 2: Percentage of times that a control strategy based on the proposed indexes was better than another control strategy in an ensemble of 100 simulations. The first column is the type of graph used in the simulations, the second column indicates whether Absolute Final Size index (AFS) or Relative Final Size index (RFS) were used. The third column indicates the alternative strategy to which the proposed strategy was compared. The random patch strategy consists of selecting a random patch to apply the control. The most connected patch strategy consists of selecting the highly connected path to applied the control. The fourth column is the percentage of times the control strategy based on AFS or RFS outperforms the alternative strategy when there is low mobility between patches. The fifth column is the percentage of times the control strategy based on AFS or RFS index outperforms the alternative strategy when there is high mobility between patches.

forms of selecting and controlling bluea patch: a selection guided by the AFS (or RFS) index, a random selection, and bluea selection of the most connected patch. We bluealso consider two different algorithms to construct graphs: the bluegraph proposed by M.E.J. Newman and D. Watts (NWG), and bluethe one proposed by R. Albert and A.L. Barabási (BAG). The control strategies guided by the AFS and RFS blueindexes are the bluemost appropriate when human mobility is low, as Table 2 blueshows. We hypothesize that low human mobility enhances the effects of the network bluestructure in the propagation of

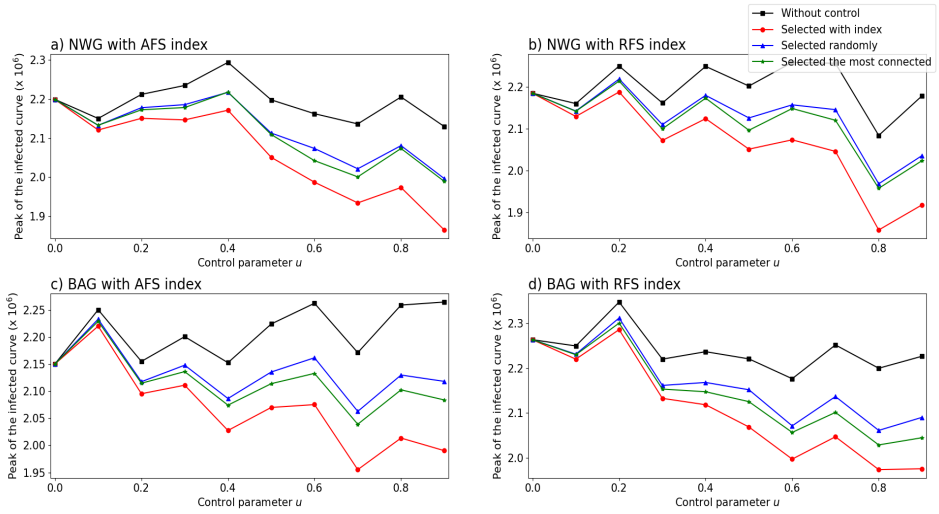

Figure 8: bluePeak epidemic size of the entire network for different values of control parameter u. In Figures (a) and (b) we observe that the control applied in the patches selected by the AFS and RFS indices better reduce the epidemic globally in the NWG network, while in Figures (c) and (d) we show that something similar is true but this time when the network has a BAG structure.

the disease, thus a strategy that takes this structure and demographic inhomogeneities into account outperforms the others. blueMoreover, the population differences in each patch lose bluerelevance at high mobility, making simpler strategies bluethat ignore this factor more efficient, blueeven though the peak of infected individuals in the entire network is not always reduced. Our results show that bluein many cases, strategies based on bluethese indexes can reduce the blueoutbreak impact on the most affected regions. blueHowever, recent experiences have shown that strategies to reduce the epidemic globally are not always the most effective. This is bluedue to the fact that health services may be bluelocally saturated. In this blueregard, since the AFS and RFS indexes are local indicators of the disease's severity, they can be employed to locate patches where health systems are prone to be saturated. It is bluetherefore reasonable to bluededuce that local health infrastructure is proportional, or at least related, blueto the local population. Thus, bluedespite the slightly better

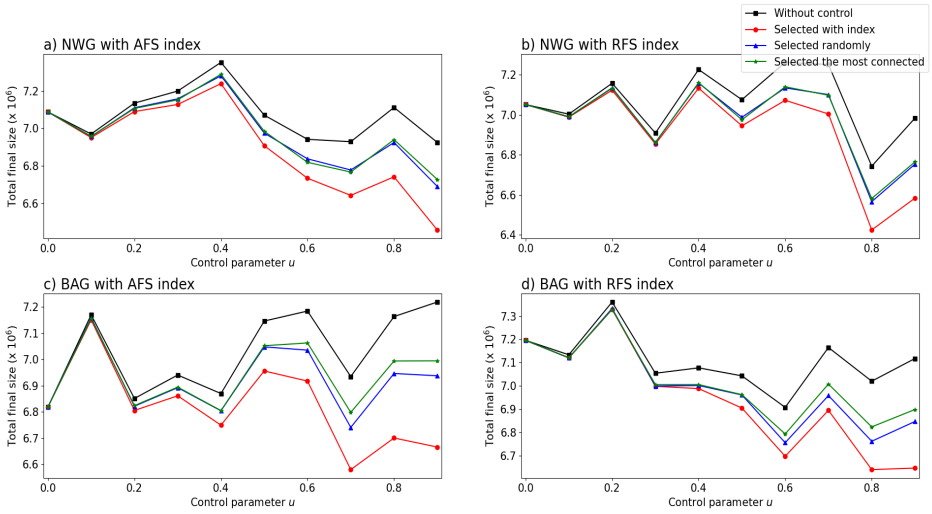

Figure 9: blueFinal size of the epidemic on the entire network for different values of control parameter u. In Figures (a) and (b) we observe that the control applied in the patches selected by the AFS and RFS indices better reduce the epidemic globally in the NWG network, while in Figures (c) and (d) we show that something similar is true but this time when the network has a BAG structure.

performance of the AFS index over the RFS index, the latter can be used to identify locations with low health care capacity bluethat are in danger of being overwhelmed.

We expect that more complex strategies that combine the AFS and RFS indexes could generate bluemore balanced strategies, where the number of infected individuals in the most contagious regions can be reduced without neglecting the most vulnerable localities due to their inability to take care for the sick. We believe that a topic for future research could consider the analysis of a control strategy that uses the AFS and RFS indexes bluein a combined form.

Acknowledgment

Authors U.J. Giménez-Mujica and A. Anzo-Hernández acknowledge CONACYT financial support through scholarship program and “Cátedras CONACYT para Jóvenes Investigadores 2016” (project 278).

Structural properties of the NWG network in the low mobility scenario.			
Selection method	**Degree**	**Clustering**	**Betweeness centrality**
AFS	5	0.451314286	0.060282091
Random (AFS)	5	0.452268254	0.057029889
M Connect (AFS)	7	0.344693651	0.134575073
RFS	5	0.446650794	0.056686845
Random (RFS)	5	0.44364127	0.058447134
M Connect (RFS)	7	0.340757143	0.134926258

Table 3: blueComparison of some structural properties between the patches selected with the AFS and RFS indices, the patches chosen at random, and the most connected patch of the network in a low mobility scenario. The results are based on the average of the sum of all the runs for each value of the control parameter $u = 0, \ldots, 9$ in an assembly of 50 simulations for each value of u.

Appendix A.

We present the proof of proposition (1), which uses standard results of the real analysis in $\mathbb{R}$ and $\mathbb{R}^n$ of metric spaces in convergence of bounded monotonic sequence.

Proof of Proposition 1. By induction, we prove that the sequence $(X^m)_{m\in\mathbb{N}}$, with $X^{k+1} = F(X^k)$ and initial condition $X^0 = (1, \cdots, 1)^T \in \mathbb{R}^n$, $\forall k > 1$ and $m \geq 1$, is monotonic increasing. At what follows, $X^k \leq X^{k+1}$ means that its corresponding entries satisfy $x_i^k \leq x_i^{k+1}$, for all $i \in \{1, \ldots, n\}$.

Base step: We proof that $X^0 \leq X^1$; where $X^1 = (x_1^1, \ldots, x_n^1)^T \in \mathbb{R}^n$, with $x_i^1 = N_i - S_i(0)e^{-\theta_i^0}$ and $\theta_i^0 = C_1 x_1^0 + \cdots + C_n x_n^0$, for $i = 1, \ldots, n$.

Since $\{C_l\}_{l=1}^n$ is a set of positive constants and the initial condition is $X^0 = (1, \cdots, 1)^T$, the term θ_i^0 satisfy:

$$\begin{aligned} \theta_i^0 = C_1 \cdot 1 + \cdots + C_n \cdot 1 > 0 \quad &\Longrightarrow \quad e^{-\theta_i^0} < 1\,, \\ &\Longrightarrow \quad (N_i - I_i(0))e^{-\theta_i^0} < N_i - I_i(0)\,, \\ &\Longrightarrow \; I_i(0) < N_i - (N_i - I_i(0))e^{-\theta_i^0}\,. \end{aligned}$$

Structural properties of the BAG network in the low mobility scenario.			
Selection method	**Degree**	**Clustering**	**Betweeness centrality**
AFS	3	0.404329004	0.07302829
Random (AFS)	3	0.368893595	0.072928162
M Connect (AFS)	8	0.166626374	0.402325477
RFS	3	0.357562093	0.069504309
Random (RFS)	3	0.385520779	0.070306525
M Connect (RFS)	8	0.168111655	0.393976366

Table 4: blueComparison of some structural properties between the patches selected with the AFS and RFS indices, the patches chosen at random, and the most connected patch of the network in a low mobility scenario. The results are based on the average of the sum of all the runs for each value of the control parameter $u = 0, \ldots, 9$ in an assembly of 50 simulations for each value of u.

But $S_i(0) = N_i - I_i(0)$ and $I_i(0) \geq 1$; then

$$1 \leq I_i(0) < N_i - S_i(0)e^{-\theta_i^0} = x_i^1 \quad \forall i \in \{1, \ldots, n\}.$$

Therefore, $1 = x_i^0 \leq x_i^1$ for all the entries of X^0 and X^1 respectively; then $X^0 \leq X^1$.

Inductive hypothesis: Assume that $X^k \geq X^{k-1}$.

Induction step: We will show that $X^{k+1} \geq X^k$. The inductive hypothesis implies that $x_i^k - x_i^{k-1} > 0$, for $i = 1, \ldots, n$. Since $\{C_l\}_{l=1}^n$ is a set of positive constants, the summatory of the terms $C_i(x_i^k - x_i^{k-1})$ satisfy

$$\begin{aligned}
&C_1(x_1^k - x_1^{k-1}) + \cdots + C_n(x_n^k - x_n^{k-1}) \geq 0\,, \\
&\implies C_1x_1^k + \cdots + C_nx_n^k \geq C_1x_1^{k-1} + \cdots + C_nx_n^{k-1}\,, \\
&\implies \theta_i^k \geq \theta_i^{k-1}\,, \\
&\implies e^{-\theta_i^k} \leq e^{-\theta_i^{k-1}}\,.
\end{aligned}$$

Multiplying $-S_i(0)$ and summing N_i both sides, we get

$$N_i - S_i(0)e^{-\theta_i^k} \geq N_i - S_i(0)e^{-\theta_i^{k-1}} \implies x_i^{k+1} \geq x_i^k\,.$$

Therefore, $X_i^{k+1} \geq X_i^k$.

Hence the sequence $(X^k)_{k\in\mathbb{N}}$ is monotonic increasing. The above also implies that every entry of X^k is positive, then, from blueEq. (15) we get that $x_i^k < N_i$, $\forall i \in \{1,\ldots,n\}$; that is, each entry i of X^k is bounded superiorly by N_i, with this we conclude that $(X^k)_{k\in\mathbb{N}}$ converge. □

Appendix B.

We propose a methodology to prove the existence and uniqueness of the solution of Eq. (14) which implies that $R_i(\infty)$ is the limit of the iteration convergence of Eq. (17). The key idea of our methodology is to posing the existence and uniqueness of the solution of Eq. (14) as an equivalent fixed point problem.

By rewriting Eq. (14) as $S_i(0)e^{-\theta_i} = N_i - R_i(\infty) > 0$, for $i = 1,\ldots,n$, and defining the number of individuals who do not contract the disease in patch i as $y_i = N_i - R_i(\infty)$, the system of equations (14) can be written as a fixed point problem for the vector function $g = (g_1,\ldots,g_n)$ given by

$$g_i(Y) = \alpha_i e^{\sum_{j=1}^n \beta_{ij}\frac{y_j}{\gamma_j}} \tag{B.1}$$

with

$$\alpha_i = S_i(0)e^{-\sum_{j=1}^n \beta_{ij}\frac{N_j}{\gamma_j}}, \quad \text{for} \quad i = 1,\ldots,n\,.$$

That is, the system of equations (14) can be rewritten as a vector equation of the form $g_i(Y)$, with $Y = (y_1,\ldots,y_n)$; then, proving the existence of a solution of the system of equations (14) is equivalent to proving the existence of a fixed point for $g_i(Y)$. For this propose, the following theorem could be used:

Theorem Appendix B.1. *Burden & Faires (2001)[Theorem 10.6] Let* $D = \{(y_1, y_2, \ldots, y_n)^t |\, a_i \leq y_i \leq b_i\,, \text{for each } i = 1,2,\ldots,n\}$ *for some collection of constants* $a_1, a_2, \ldots, a_n$ *and* $b_1, b2, \ldots, b_n$. *Suppose* g *is a continuous function from* $D \subset \mathbb{R}^n \longrightarrow \mathbb{R}^n$ *with the property that* $g(Y) \in D$ *whenever* $Y \in D$. *Then*

g has a fixed point in D.

Moreover, suppose that all the component functions of g have continuous partial derivatives and a constant $q < 1$ *exists with*

$$\left|\frac{\partial g_i(Y)}{\partial y_j}\right| \leq \frac{q}{n}, \qquad \textit{whenever } Y \in D,$$

for each $j = 1, 2 \ldots, n$ *and each component function* g_i. *Then the sequence* $(Y^{(k)})_{k=0}^{\infty}$, *defined by an arbitrarily selected* $Y^{(0)}$ *in* D *and generated by*

$$Y^{(k)} = g(Y^{(k-1)}), \qquad \textit{for each } k \geq 1$$

converges to the unique fixed point $y^* \in D$ *and*

$$\| y^{(k)} - y^* \| \leq \frac{q^k}{1-q} \| y^{(1)} - y^{(0)} \| .$$

When we calculate the Jacobian matrix of the functional $g_i(Y)$ we get:

$$J_g(Y) = Ag(Y), \tag{B.2}$$

where A is a matrix whose elements are:

$$a_{il} = \left(\sum_{k=1}^{n} \frac{\beta^k p_{ik} p_{lk}}{\gamma_l w_k} \right). \tag{B.3}$$

Then, by imposing or finding the adequate conditions on the elements of the matrix A so the hypotheses of the Theorem (Appendix B.1) are satisfied, we could set the set parameter values that guarantee the existence and uniqueness of a fixed point and thus have a unique solution of the blueEq. (14).

We consider that this problem requires meticulous analysis worth of investigation in future research works.

References

Angelo, K. M., Gastañaduy, P. A., Walker, A. T., Patel, M., Reef, S., Lee, C. V., & Nemhauser, J. (2019). Spread of measles in europe and implications for US travelers. *Pediatrics*, *144*, e20190414.

Balcan, D., & Vespignani, A. (2012). Invasion threshold in structured populations with recurrent mobility patterns. *Journal of Theoretical Biology*, *293*, 87–100.

Barabási, A.-L., & Albert, R. (1999). Emergence of scaling in random networks. *Science*, *286*, 509–512.

Bichara, D., Kang, Y., Castillo-Chavez, C., Horan, R., & Perrings, C. (2015). SIS and SIR Epidemic Models Under Virtual Dispersal. *Bulletin of Mathematical Biology*, *77*, 2004–2034.

Brauer, F., Castillo-Chavez, C., & Feng, Z. (2019). *Mathematical Models in Epidemiology*. Springer New York.

Burden, R. L., & Faires, J. D. (2001). *Numerical Analysis*. CENGAGE Learning, Boston.

Chinazzi, M., Davis, J. T., Ajelli, M., Gioannini, C., Litvinova, M., Merler, S., y Piontti, A. P., Mu, K., Rossi, L., Sun, K., Viboud, C., Xiong, X., Yu, H., Halloran, M. E., Longini, I. M., & Vespignani, A. (2020). The effect of travel restrictions on the spread of the 2019 novel coronavirus (COVID-19) outbreak. *Science*, (p. eaba9757).

Colizza, V., & Vespignani, A. (2008). Epidemic modeling in metapopulation systems with heterogeneous coupling pattern: Theory and simulations. *Journal of Theoretical Biology*, *251*, 450–467.

Ding, R. (2019). The complex network theory-based urban land-use and transport interaction studies. *Complexity*, *2019*, 1–14.

Fraser, C., Donnelly, C., Cauchemez, S., Hanage, W., Van Kerkhove, M., Hollingsworth, T., Griffin, J., Baggaley, R., Jenkins, H., Lyons, E., Jombart, T., Hinsley, W., Grassly, N., Balloux, F., Ghani, A., Ferguson, N., Rambaut, A., Pybus, O., Lopez-Gatell, H., & Roth, C. (2009). Pandemic potential of a strain of influenza a (h1n1): Early findings. *Science (New York, N.Y.)*, *324*, 1557–61.

Guida, M., & Maria, F. (2007). Topology of the italian airport network: A scale-free small-world network with a fractal structure? *Chaos, Solitons & Fractals*, *31*, 527–536.

Lee, J., Choi, B. Y., & Jung, E. (2018). Metapopulation model using commuting flow for national spread of the 2009 h1n1 influenza virus in the republic of korea. *Journal of Theoretical Biology*, *454*, 320–329.

Lee, J. M., Choi, D., Cho, G., & Kim, Y. (2012). The effect of public health interventions on the spread of influenza among cities. *Journal of Theoretical Biology*, *293*, 131–142.

Magal, P., Seydi, O., & Webb, G. (2018). Final size of a multi-group SIR epidemic model: Irreducible and non-irreducible modes of transmission. *Mathematical Biosciences*, *301*, 59–67.

Mansilla, R., & Mendozas, R. (2010). The network of mexican cities. *arXiv: Adaptation and Self-Organizing Systems*, .

Martcheva, M. (2015). *An Introduction to Mathematical Epidemiology*. Springer New York.

Miller, J. C. (2012). A note on the derivation of epidemic final sizes. *Bulletin of Mathematical Biology*, *74*, 2125–2141.

Newman, M., & Watts, D. (1999). Renormalization group analysis of the small-world network model. *Physics Letters A*, *263*, 341–346.

Pastor-Satorras, R., Castellano, C., Mieghem, P. V., & Vespignani, A. (2015). Epidemic processes in complex networks. *Reviews of Modern Physics*, *87*, 925–979.

Velázquez-Castro, J., Anzo-Hernández, A., Bonilla-Capilla, B., Soto-Bajo, M., & Fraguela-Collar, A. (2018). Vector-borne disease risk indexes in spatially structured populations. *PLOS Neglected Tropical Diseases*, *12*, e0006234.

Volchenkov, D., & Blanchard, P. (2008). Comparative study of cities as complex networks. *arXiv: Physics and Society*, .